Phase behavior of the system hyperbranched polyglycerol+methanol+carbon dioxide

ARTICLE *in* FLUID PHASE EQUILIBRIA · DECEMBER 2010

Impact Factor: 2.2 · DOI: 10.1016/j.fluid.2010.09.028

6 AUTHORS, INCLUDING:

Holger Frey
Johannes Gutenberg-Universität Mainz
364 PUBLICATIONS **10,426** CITATIONS
SEE PROFILE

Joachim Gross
Universität Stuttgart
90 PUBLICATIONS **2,884** CITATIONS
SEE PROFILE

Fluid Phase Equilibria 299 (2010) 252–258

Contents lists available at ScienceDirect

Fluid Phase Equilibria

journal homepage: www.elsevier.com/locate/fluid

Phase behavior of the system hyperbranched polyglycerol + methanol + carbon dioxide

Christian S. Schacht[a], Sara Bahramali[a], Daniel Wilms[c], Holger Frey[c], Joachim Gross[a,b], Theo W. de Loos[a,*]

[a] Engineering Thermodynamics, Process & Energy Department, Delft University of Technology, Delft, The Netherlands
[b] Institute of Thermodynamics and Thermal Process Engineering, University of Stuttgart, Stuttgart, Germany
[c] Institute of Organic Chemistry, Johannes Gutenberg-University Mainz, Mainz, Germany

ARTICLE INFO

Article history:
Received 5 July 2010
Received in revised form
20 September 2010
Accepted 21 September 2010
Available online 29 September 2010

Keywords:
Hyperbranched polymer
PC-SAFT equation of state
Liquid–liquid
Vapor–liquid
Liquid–liquid–vapor

ABSTRACT

Phase equilibrium data have been measured for the ternary system hyperbranched polyglycerol + methanol + carbon dioxide at temperatures of 313–450 K and pressures up to 13.5 MPa. Phase changes were determined according to a synthetic method using the Cailletet setup. At elevated temperatures the system shows a liquid–liquid–vapor region with lower solution temperatures. Besides the vapor–liquid and liquid–liquid equilibria, the vapor–liquid to vapor–liquid–liquid and vapor–liquid–liquid to liquid–liquid phase boundaries are reported at different polymer molar masses and can serve as test sets for thermodynamic models. A distinct influence of the polymer molar mass on the vapor–liquid equilibrium can be noticed and indicates the existence of structural effects due to the polymer branching. Modeling the systems with the PCP-SAFT equation of state confirms these findings.

1. Introduction

Recent advances in polymer technology allow for the efficient one-pot production of highly branched polymers [1]. These hyperbranched polymers do not only exhibit viscosities far below their linear analogues [2,3], but also offer many degrees of freedom (degree of branching, molecule size, number and kind of functional groups, differentiation between core and shell groups) to specifically tune their interactions with other compounds. These qualities inspired scientists to use hyperbranched polymers as designer solvents or entrainer for extraction, extractive distillation as well as absorption processes. Sorption experiments with dendrimers already pointed out, that highly branched compounds have a higher absorptive capacity than their linear analogues, probably due to a lower degree of crystallization [4]. The work of Seiler et al. [5–9] demonstrated that the ethanol–water azeotrope can be overcome by the addition of hyperbranched polyglycerol. Rolker et al. [10] showed the advantage of applying hyperbranched polymers as solvents for carbon dioxide capture. The high viscosity of the material suggests the use of co-solvents. Kozlowska et al. [11] studied the application of hyperbranched polyclycerols + alkanol mixtures for pre-combustion carbon capture.

The rheological properties of hyperbranched polymers as well as of dendrimers strongly depend on their generation number which corresponds to their molar mass [12,13]. This raises the question in how far solvent properties such as a compound's solubility is affected by the polymer molar mass. The work of Lieu et al. [14] confirmed the strong influence of molecule size on the vapor–liquid equilibria of dendritic systems, whereas, a similar systematic analysis is still missing for hyperbranched polymers. Such an investigation might have been impeded by the broad size distribution that different samples of hyperbranched polymers usually exhibit. Among hyperbranched polymers with branch-on-branch type topology, only few systems permit the synthesis of materials with controlled molecular mass and low polydispersity. In the case of hyperbranched polyglycerol, molecular masses ranging between 500 g/mol and 100,000 g/mol are currently available [15]. Only recently, Wilms et al. [16] succeeded in synthesizing high molar mass HBP at polydispersities (M_w/M_n) as low as 1.5, offering a product that is sufficiently characterized for investigating the influence of polymer molar mass on the phase equilibrium. Apart from phase equilibrium data, also thermodynamic models to describe these systems are required to develop processes including HBPs. The numerous hydroxy groups per molecule allow for tailoring the polymer according to its application via a second synthesis step [15]. Mainly, three approaches have been followed to account for the three-dimensional structure of molecules within thermodynamic models. For low pressure applications' the lattice

* Corresponding author. Tel.: +31 15 2786651; fax: +31 15 2782460.
E-mail addresses: T.W.deLoos@TUDelft.nl, fpe-3me@tudelft.nl (T.W. de Loos).

0378-3812/$ – see front matter © 2010 Elsevier B.V. All rights reserved.
doi:10.1016/j.fluid.2010.09.028

cluster theory (LCT) [4,14,17–21] as well as the free volume UNIFAC (UNIFAC-FV) give good agreement with experimental data. In view of processes at higher pressure, the use of the PCP SAFT equation of state for branched molecules (bPCP SAFT) as proposed by Kozlowska et al. [11] can be advantageous. However, with this equation, the liquid–liquid demixing in the system hyperbranched polyglycerol + methanol + carbon dioxide is predicted at too high temperatures [11].

In this work, phase equilibrium data of the system hyperbranched polyglycerol + methanol + carbon dioxide is given over a large range of polymer molar masses and the influence of the polymer size on the phase envelope is investigated. On the other hand, the bPCP SAFT equation of state is re-parameterized to describe the liquid–liquid equilibria of the system.

2. Experimental

2.1. Materials and sample preparation

Hyperbranched polyglycerols (HPG) of 5700 (M_w/M_n = 1.7), 10,000 (M_w/M_n = 1.4) and 18,000 g/mol (M_w/M_n = 1.4) have been used in this work. All samples are liquids of high viscosity at room temperature. These HPG's have been prepared in one or two synthesis steps according to recently published procedures [16]. The degrees of branching of the HBP are in the range of 0.55–0.6 and the chemical structure can be seen in Fig. 1. The molar mass distributions have been determined by GPC with polystyrene standards. A detailed analysis on the use of this method in combination with hyperbranched polymer systems can be found elsewhere [16].

The carbon dioxide was obtained from Hoek Loos with a minimum purity of 99.995%. Methanol with a purity of 98.5% was purchased from J.T. Baker. A mixture of hyperbranched polyglycerol and methanol is prepared and filled into the Cailletet tube. The masses are determined with an analytical balance. The mixture is degassed by repeated freezing and melting under vacuum. Carbon dioxide is added to the sample by using a gas-volumetric method. The mass of carbon dioxide is determined with the virial equation truncated after the second term. Uncertainties within the components' mass are below ±0.0001 g, with a typical sample size around 0.1 g. The water content of the samples is given in Table 1. Measurements for HPG(5700 g/mol) + methanol + CO_2 with varying water content (below 1 mass-%) were invariant within the experimental accuracy with respect to the bubble and cloud point pressures.

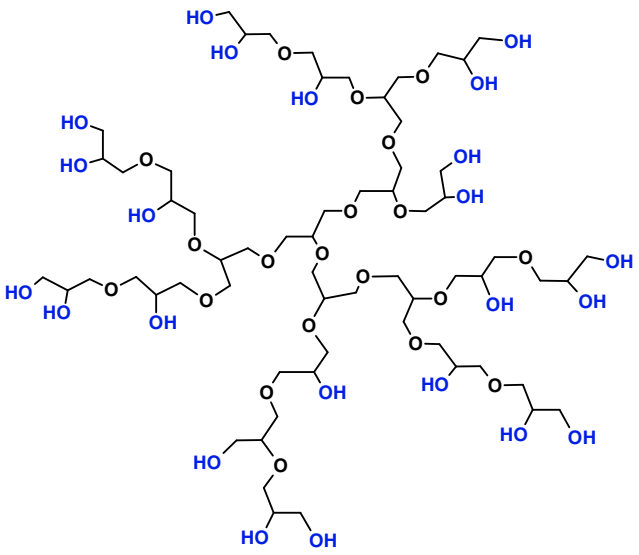

Fig. 1. Chemical structure of polyglycerol.

Table 1
Water content of the samples.

System (numbers indicate mass fractions)	Water content (ppm)
(0.977) · [0.501 · HPG(10 kg/mol) + 0.499 · CH_3OH] + 0.023 · CO_2	2326
(0.953) · [0.501 · HPG(10 kg/mol) + 0.499 · CH_3OH] + 0.047 · CO_2	1649
(0.902) · [0.501 · HPG(10 kg/mol) + 0.499 · CH_3OH] + 0.098 · CO_2	1649
(0.849) · [0.501 · HPG(10 kg/mol) + 0.499 · CH_3OH] + 0.151 · CO_2	2326
(0.980) · [0.248 · HPG(10 kg/mol) + 0.752 · CH_3OH] + 0.020 · CO_2	2516
(0.953) · [0.248 · HPG(10 kg/mol) + 0.752 · CH_3OH] + 0.047 · CO_2	1611
(0.902) · [0.248 · HPG(10 kg/mol) + 0.752 · CH_3OH] + 0.098 · CO_2	549
(0.855) · [0.248 · HPG(10 kg/mol) + 0.752 · CH_3OH] + 0.145 · CO_2	1382
(0.979) · [0.499 · HPG(18 kg/mol) + 0.501 · CH_3OH] + 0.021 · CO_2	542
(0.941) · [0.502 · HPG(18 kg/mol) + 0.498 · CH_3OH] + 0.059 · CO_2	782
(0.895) · [0.500 · HPG(18 kg/mol) + 0.500 · CH_3OH] + 0.105 · CO_2	1370
(0.855) · [0.500 · HPG(18 kg/mol) + 0.500 · CH_3OH] + 0.145 · CO_2	1713
(0.979) · [0.250 · HPG(18 kg/mol) + 0.750 · CH_3OH] + 0.021 · CO_2	243
(0.951) · [0.250 · HPG(18 kg/mol) + 0.750 · CH_3OH] + 0.049 · CO_2	243
(0.898) · [0.250 · HPG(18 kg/mol) + 0.750 · CH_3OH] + 0.102 · CO_2	645
(0.849) · [0.250 · HPG(18 kg/mol) + 0.750 · CH_3OH] + 0.151 · CO_2	696

2.2. Phase equilibrium measurements

The phase equilibria are determined by a static-synthetic method using the Cailletet apparatus. A detailed description of the experimental setup can be found elsewhere [22]. Phase changes are determined visually by pressure adjustments at constant temperature. Pressures are measured with a dead weight gauge at an accuracy of ±0.005 MPa. Temperature measurements are taken with a platinum resistance thermometer at an accuracy of ±0.02 K. The PID control allows for keeping the temperatures in a range of ±0.02 K with silicone oil as the thermostat liquid.

3. Results and discussion

3.1. Experimental results

To identify the influence of the polyglycerol molecule size and, thus, the molar mass of the hyperbranched polyglycerol (HPG) on the phase behavior of the system HPG + methanol + carbon dioxide, samples with varying molar mass of HBP were investigated. The experimental results are given in Tables 2–7. The bubble-point curves of mixtures containing hyperbranched PG with 5700 g/mol, 10,000 g/mol and 18,000 g/mol were determined at two different ratios of HBP to methanol with varying carbon dioxide concentrations.

Fig. 2 shows the pressure–temperature phase envelope for the system hyperbranched polyglycerol (5700 g/mol) + methanol + carbon dioxide. Demixing of the liquid phase occurs at elevated temperatures leading to the formation of a liquid–liquid–vapor region and at higher pressure a liquid–liquid region with lower solution temperatures (LST). The liquid–liquid region is separated from the homogeneous liquid region by the cloud point curve. The LST shifts to lower temperatures and higher pressures with increasing carbon dioxide concentration. This behavior has been described earlier [11,23] and has also been found for hyperbranched polyester + ethanol + carbon dioxide systems [6]. As discussed in Ref. [11] the system can be identified as a type IV system according to the fluid phase behavior classification of Konynenburg and Scott [24]. The systems including polymer with higher molar mass show a similar behavior as can be seen in Fig. 3. In this diagram only bubble and cloud point curves are given. The effect of polymer concentration on the phase behavior can be seen in Fig. 4.

Hyperbranched polyglycerol + methanol + carbon dioxide systems show a significant increase of the bubble-point pressure

Table 2
Experimental bubble point (VL), cloud point (LL), phase boundary vapor–liquid to liquid–liquid–vapor (LLV) and phase boundary liquid–liquid–vapor to liquid–liquid (LVL) data for $w_1 \cdot CO_2 + (1 - w_1)[w_2 \cdot HPG(5700\,g/mol) + w_3 \cdot CH_3OH]$ at various mass fractions w_1 of CO_2, for $w_2 = 0.499$ and $w_3 = 0.501$.

$w_1 = 0.020$		$w_1 = 0.050$		$w_1 = 0.100$		$w_1 = 0.150$	
T (K)	P (MPa)	T (K)	P (MPa)	T (K)	P (MPa)	T (K)	P (MPa)
332.70	0.941 (VL)	332.66	2.218 (VL)	332.99	4.330 (VL)	333.00	5.281 (LLV)
342.47	1.081 (VL)	342.41	2.523 (VL)	343.00	4.691 (VL)	343.01	5.917 (LLV)
352.20	1.246 (VL)	352.12	2.867 (VL)	353.03	5.611 (VL)	353.04	6.517 (LLV)
361.89	1.407 (VL)	352.17	2.848 (VL)	363.03	6.282 (VL)	363.05	7.058 (LLV)
371.57	1.594 (VL)	361.82	3.202 (VL)	373.04	6.952 (VL)	373.07	7.518 (LLV)
381.29	1.812 (VL)	361.89	3.183 (VL)	383.03	7.633 (VL)	383.05	7.899 (LLV)
390.99	2.042 (VL)	371.57	3.552 (VL)	393.04	8.053 (LLV)	393.18	8.179 (LLV)
400.73	2.317 (VL)	371.57	3.539 (VL)	403.07	8.198 (LLV)	403.13	8.340 (LLV)
410.48	2.622 (VL)	381.29	3.914 (VL)	408.02	8.198 (LLV)	333.00	6.271 (LVL)
420.26	2.978 (VL)	381.31	3.933 (VL)	413.02	8.239 (LLV)	343.01	7.132 (LVL)
		390.88	4.398 (VL)	423.02	8.179 (LLV)	353.04	8.012 (LVL)
		400.76	4.818 (VL)	433.05	8.059 (LLV)	363.05	8.853 (LVL)
		410.51	5.268 (VL)	442.99	8.039 (LLV)	373.07	9.684 (LVL)
		420.27	5.768 (VL)	452.85	7.799 (LVL)	393.18	11.239 (LVL)
		439.79	6.879 (VL)	403.02	8.873 (LVL)	403.13	11.855 (LVL)
		449.55	7.494 (VL)	408.02	9.134 (LVL)		
				413.02	9.439 (LVL)		
				423.02	9.974 (LVL)		
				433.05	10.505 (LVL)		
				443.00	11.050 (LVL)		
				452.87	11.476 (LVL)		
				393.04	9.454 (VL)		
				403.05	12.141 (VL)		
				408.02	13.461 (VL)		

with increasing polymer molar mass (see Fig. 5). According to Flory–Huggins theory, the bubble-point pressure of a typical polymer solution converges with increasing molar mass at constant temperature and composition [25]. Seemingly, the hyperbranched polyglycerol system deviates from Flory–Huggins theory, which suggests a structural effect taking place, possibly, due to the crowding of functional groups in the shell of the polyglycerol molecule. This assumption is supported by the observation that upon crossing the liquid–liquid phase boundary the lower phase (polymer rich phase) builds up with increasing temperature for all samples investigated, i.e., the concentration at the lower critical solution temperature exceeds polymer mass fractions of $w_{polymer} = 0.45$. Usual polymer systems of comparable molar mass exhibit a critical polymer concentration of $w_{polymer} = 0.1$ to $w_{polymer} = 0.2$ [26].

3.2. Modeling with PCP-SAFT equation of state

The PC-SAFT equation of state [27–29] has recently been extended to polar mixtures [30,31] and has been successfully applied to model polymer [32], copolymer [33] and hyperbranched polymer [11] systems. With the parameterization of the branched PCP-SAFT equation of state as given in [11] the LST is, usually, given at temperatures significantly above the experimental values. This behavior is likely to be caused by an overestimation of the intermolecular hydrogen bonding, as the associative parameters were taken from butanol according to an analogy described in Ref. [11]. We, therefore, readjusted the association volume $\kappa^{A_iB_j}$ and the dispersive energy ε_i/k_B and allowed the binary interaction parameters k_{ij} to be linearly dependent on temperature. The parameters were determined by a simultaneous least square optimization

Table 3
Experimental bubble point (VL), cloud point (LL), phase boundary vapor–liquid to liquid–liquid–vapor (LLV) and phase boundary liquid–liquid–vapor to liquid–liquid (LVL) data for $w_1 \cdot CO_2 + (1 - w_1)[w_2 \cdot HPG(5700\,g/mol) + w_3 \cdot CH_3OH]$ at various mass fractions w_1 of CO_2, for $w_2 = 0.250$ and $w_3 = 0.750$.

$w_1 = 0.020$		$w_1 = 0.050$		$w_1 = 0.100$		$w_1 = 0.150$	
T (K)	P (MPa)	T (K)	P (MPa)	T (K)	P (MPa)	T (K)	P (MPa)
332.86	0.641 (VL)	333.11	1.457 (VL)	313.10	1.961 (VL)	332.73	4.234 (LVL)
342.54	0.742 (VL)	343.09	1.672 (VL)	323.09	2.301 (VL)	342.10	4.769 (LVL)
352.22	0.858 (VL)	353.12	1.902 (VL)	333.12	2.639 (VL)	351.70	5.303 (LVL)
361.90	0.993 (VL)	363.14	2.149 (VL)	353.15	3.452 (VL)	351.81	5.314 (LVL)
371.56	1.148 (VL)	373.16	2.413 (VL)	373.24	4.288 (VL)	361.53	5.878 (LVL)
381.24	1.328 (VL)	383.15	2.745 (VL)	393.18	5.177 (VL)	371.26	6.451 (LVL)
390.96	1.528 (VL)	393.15	3.052 (VL)	398.13	5.396 (VL)	371.29	6.440 (LVL)
400.68	1.768 (VL)	403.14	3.381 (VL)	403.15	5.637 (VL)	380.93	6.996 (LVL)
405.65	1.888 (VL)	413.14	3.705 (VL)	413.10	6.113 (VL)	380.99	6.985 (LVL)
410.45	2.043 (VL)	423.09	4.116 (VL)	423.06	6.613 (VL)	390.59	7.508 (LVL)
420.19	2.366 (VL)	433.07	4.573 (VL)	433.00	6.750 (LLV)	400.20	8.017 (LVL)
429.91	2.734 (VL)			442.97	6.391 (LLV)	409.83	8.522 (LVL)
439.66	3.161 (VL)			452.92	5.952 (LLV)	419.46	9.012 (LVL)
449.37	3.889 (VL)			433.00	7.105 (LVL)	428.38	9.492 (LVL)
				442.96	7.606 (LVL)	438.76	9.977 (LVL)
				452.89	8.141 (LVL)	448.40	10.448 (LVL)
				433.00	8.156 (LL)		
				442.95	10.998 (LL)		

Table 4
Experimental bubble point (VL), cloud point (LL), phase boundary vapor–liquid to liquid–liquid–vapor (LLV) and phase boundary liquid–liquid–vapor to liquid–liquid (LVL) data for $w_1 \cdot CO_2 + (1 - w_1)[w_2 \cdot HPG(10,000\,g/mol) + w_3 \cdot CH_3OH]$ at various mass fractions w_1 of CO_2, for $w_2 = 0.501$ and $w_3 = 0.499$.

$w_1 = 0.023$		$w_1 = 0.047$		$w_1 = 0.098$		$w_1 = 0.151$	
T (K)	P (MPa)	T (K)	P (MPa)	T (K)	P (MPa)	T (K)	P (MPa)
312.25	0.993 (VL)	312.25	1.804 (VL)	313.30	3.311 (LLV)	332.14	6.715 (LVL)
317.49	1.078 (VL)	322.16	2.089 (VL)	318.19	3.592 (LLV)	342.07	7.665 (LVL)
322.18	1.168 (VL)	332.12	2.409 (VL)	323.18	3.837 (LLV)	351.83	8.572 (LVL)
326.92	1.258 (VL)	342.01	2.764 (VL)	333.06	4.412 (LLV)	361.84	9.492 (LVL)
332.06	1.354 (VL)	351.95	3.130 (VL)	342.97	4.938 (LLV)	371.72	10.378 (LVL)
337.17	1.460 (VL)	361.83	3.511 (VL)	347.91	5.228 (LLV)	380.93	11.199 (LVL)
341.98	1.559 (VL)	371.83	3.911 (VL)	352.87	5.478 (LLV)		
346.77	1.674 (VL)	381.81	4.327 (VL)	357.83	5.733 (LLV)		
351.95	1.779 (VL)	391.74	4.777 (VL)	362.77	5.959 (LLV)		
356.69	1.904 (VL)	401.65	5.242 (VL)	372.65	6.364 (LLV)		
361.78	2.014 (VL)	411.61	5.742 (VL)	382.53	6.699 (LLV)		
366.60	2.146 (VL)	421.43	6.284 (VL)	392.45	6.955 (LLV)		
371.20	2.270 (VL)	426.47	6.560 (LLV)	402.35	7.105 (LLV)		
381.09	2.555 (VL)	431.42	6.835 (LLV)	412.26	7.165 (LLV)		
396.24	3.035 (VL)	426.47	7.175 (LL)	422.17	7.176 (LLV)		
401.35	3.205 (VL)			432.10	7.036 (LLV)		
411.19	3.591 (VL)			313.31	3.541 (LVL)		
421.16	4.011 (VL)			318.20	3.832 (LVL)		
431.00	4.486 (VL)			323.16	4.157 (LVL)		
440.91	5.032 (VL)			333.08	4.797 (LVL)		
				342.97	5.463 (LVL)		
				347.92	5.798 (LVL)		
				352.87	6.148 (LVL)		
				357.82	6.479 (LVL)		
				362.78	6.829 (LVL)		
				372.65	7.499 (LVL)		
				382.54	8.160 (LVL)		
				392.45	8.805 (LVL)		
				402.36	9.426 (LVL)		
				412.26	10.021 (LVL)		
				422.17	10.592 (LVL)		
				432.09	11.137 (LVL)		
				313.29	7.208 (LL)		
				318.18	7.724 (LL)		
				323.11	8.264 (LL)		
				328.08	8.830 (LL)		
				347.87	11.416 (LL)		

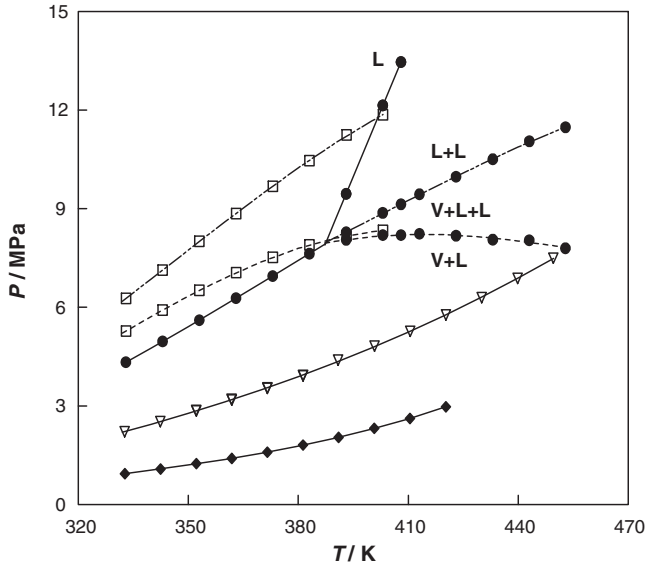

Fig. 2. Phase diagram of the ternary system $(1 - w_{CO_2})$[50 mass-% hyperbranched PG (5700 g/mol) + 50 mass-% methanol] and CO_2, with $w_{CO_2} = 0.02$ (*diamonds*), $w_{CO_2} = 0.05$ (*open triangles*), $w_{CO_2} = 0.10$ (*circles*), and $w_{CO_2} = 0.15$ (*open squares*). The lines are a guide for the eye, where solid lines indicate bubble and dew point curves, dashed lines show the VL to VLL phase boundary and dash-dotted lines are the VLL to LL phase boundary.

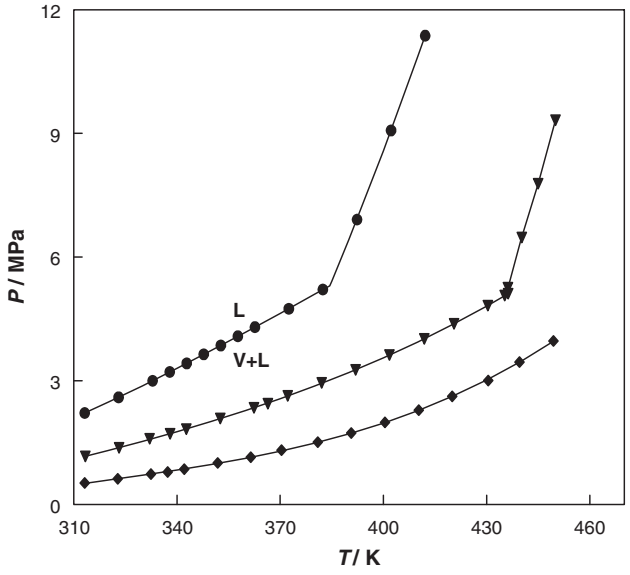

Fig. 3. Bubble and cloud point curves of the ternary system $(1 - w_{CO_2})$[25 mass-% hyperbranched PG (10,000 g/mol) + 75 mass-% methanol] and CO_2, with $w_{CO_2} = 0.02$ (*diamonds*), $w_{CO_2} = 0.05$ (*triangles*), and $w_{CO_2} = 0.10$ (*circles*). The lines are a guide for the eye.

Table 5
Experimental bubble point (VL), cloud point (LL), phase boundary vapor–liquid to liquid–liquid–vapor (LLV) and phase boundary liquid–liquid–vapor to liquid–liquid (LVL) data for $w_1 \cdot CO_2 + (1 - w_1)[w_2 \cdot HPG(10,000\,g/mol) + w_3 \cdot CH_3OH]$ at various mass fractions w_1 of CO_2, for $w_2 = 0.248$ and $w_3 = 0.752$.

$w_1 = 0.020$		$w_1 = 0.047$		$w_1 = 0.098$		$w_1 = 0.150$	
T (K)	P (MPa)	T (K)	P (MPa)	T (K)	P (MPa)	T (K)	P (MPa)
313.22	0.525 (VL)	313.37	1.167 (VL)	313.17	2.221 (VL)	313.11	3.403 (LVL)
322.81	0.626 (VL)	323.16	1.377 (VL)	323.03	2.601 (VL)	322.96	3.968 (LVL)
332.48	0.736 (VL)	332.06	1.597 (VL)	332.92	3.001 (VL)	332.86	4.574 (LVL)
337.26	0.790 (VL)	337.99	1.714 (VL)	337.87	3.216 (VL)	342.77	5.189 (LVL)
342.14	0.856 (VL)	342.71	1.833 (VL)	342.83	3.422 (VL)	352.68	5.820 (LVL)
351.83	1.006 (VL)	352.61	2.088 (VL)	347.79	3.642 (VL)	357.68	6.140 (LVL)
361.46	1.146 (VL)	362.39	2.348 (VL)	352.76	3.857 (VL)	362.59	6.450 (LVL)
370.40	1.316 (VL)	366.42	2.449 (VL)	357.71	4.082 (VL)	372.46	7.061 (LVL)
380.92	1.512 (VL)	372.20	2.639 (VL)	362.66	4.302 (VL)	382.37	7.666 (LVL)
390.65	1.737 (VL)	382.04	2.949 (VL)	372.51	4.748 (VL)	392.27	8.257 (LVL)
400.46	1.992 (VL)	391.90	3.269 (VL)	382.41	5.213 (VL)	402.16	8.832 (LVL)
410.25	2.287 (VL)	401.72	3.625 (VL)	392.32	5.404 (LLV)	412.08	9.383 (LVL)
419.99	2.623 (VL)	411.84	4.015 (VL)	402.25	5.429 (LLV)	421.99	9.923 (LVL)
430.45	3.008 (VL)	420.55	4.380 (VL)	412.16	5.379 (LLV)	431.95	10.443 (LVL)
439.53	3.454 (VL)	430.36	4.826 (VL)	422.07	5.215 (LLV)	441.89	10.969 (LLV)
449.38	3.969 (VL)	435.22	50.66 (VL)	432.04	4.946 (LLV)	313.07	2.809 (LLV)
		436.19	5.046 (LLV)	441.93	4.598 (LLV)	322.94	3.304 (LLV)
		440.24	4.861 (LLV)	451.87	4.231 (LLV)	332.88	3.70 (LLV)
		444.92	4.677 (LLV)	392.31	5.674 (LVL)	342.77	4.14 (LLV)
		450.03	4.418 (LLV)	402.22	6.144 (LVL)	352.68	4.56 (LLV)
		436.21	5.111 (LVL)	412.15	6.614 (LVL)	357.66	4.77 (LLV)
		440.23	5.306 (LVL)	422.07	7.100 (LVL)	362.58	4.93 (LLV)
		444.90	5.552 (LVL)	432.03	7.605 (LVL)	372.43	5.23 (LLV)
		450.03	5.827 (LVL)	441.96	8.126 (LVL)	382.37	5.46 (LLV)
		436.16	5.256 (LL)	451.88	8.671 (LVL)	392.27	5.60 (LLV)
		440.19	6.477 (LL)	392.31	6.914 (LL)	402.15	5.66 (LLV)
		444.94	7.778 (LL)	402.22	9.071 (LL)	412.09	5.60 (LLV)
		450.01	9.319 (LL)	412.13	11.372 (LL)	421.99	5.45 (LLV)
						431.94	5.18 (LLV)
						441.87	4.85 (LLV)

with the system $0.1CO_2 + 0.9$[50 mass-% hyperbranched PG (2700 g/mol) + 50 mass-% methanol] as given in Ref. [11] to $\kappa^{A_iB_j} = 0.0004$, $\varepsilon_i/k_B = 311$ K, $k_{HPG2,MeOH} = 60.5 \cdot e^{-5} \cdot (T/K - 320)$ and $k_{HPG2,CO_2} = 10.5 \cdot e^{-5} \cdot (T/K - 320)$. All other parameters are defined as published in Ref. [11].

The model shows good agreement with the experimental data. As can be concluded from Fig. 6 the model allows for extrapolations in carbon dioxide as well as polymer concentrations. Fig. 7 demonstrates that extrapolations in polymer molecular mass are also possible. However, the dew point behavior is not described accurately anymore at higher molar masses. Further, the model shows the upper solution temperature at temperatures below our experimental window and, therefore, in agreement with the experimental data. With temperature-dependent binary interaction parameters, we enforce the VLLE point for some systems; at the same time the slope of the LLE curve is sacrificed (compare Fig. 7). As can be seen elsewhere [32] the PC-SAFT eos is usually capable of accurately describing VLLE equilibria without the use of temperature dependent binary parameters. The fact that these systems require the use of temperature dependent binary corrections suggests, that structural effects of the hyperbranched polyglycerol are not properly accounted for within the equation of state. A structural change

Table 6
Experimental bubble point (VL), cloud point (LL), phase boundary vapor–liquid to liquid–liquid–vapor (LLV) and phase boundary liquid–liquid–vapor to liquid–liquid (LVL) data for $w_1 \cdot CO_2 + (1 - w_1)[w_2 \cdot HPG(18,000\,g/mol) + w_3 \cdot CH_3OH]$ at various mass fractions w_1 of CO_2, for $w_2 = 0.499$ and $w_3 = 0.501$.

$w_1 = 0.021$		$w_1 = 0.055$		$w_1 = 0.105$		$w_1 = 0.145$	
T (K)	P (MPa)	T (K)	P (MPa)	T (K)	P (MPa)	T (K)	P (MPa)
313.13	0.832 (VL)	313.15	1.167 (VL)	313.08	3.182 (LLV)	311.99	4.665 (LVL)
327.95	1.067 (VL)	327.93	1.377 (VL)	327.91	3.952 (LLV)	319.34	5.256 (LVL)
335.35	1.177 (VL)	342.79	1.597 (VL)	335.36	4.348 (LLV)	326.59	5.896 (LVL)
342.78	1.323 (VL)	347.77	1.714 (VL)	342.76	4.733 (LLV)	341.11	7.222 (LVL)
357.68	1.618 (VL)	357.68	1.833 (VL)	357.62	5.449 (LLV)	348.53	7.867 (LVL)
372.49	1.954 (VL)	372.46	2.088 (VL)	372.43	6.064 (LLV)	355.54	8.548 (LVL)
387.37	2.344 (VL)	387.35	2.348 (VL)	387.31	6.515 (LLV)	370.20	9.828 (LVL)
402.21	2.804 (VL)	402.23	2.449 (VL)	402.16	6.790 (LLV)	377.58	10.395 (LVL)
417.12	3.355 (VL)	417.08	2.639 (VL)	313.09	3.686 (LVL)	384.86	11.039 (LVL)
432.02	4.006 (VL)	427.06	2.949 (LLV)	327.90	4.652 (LVL)		
446.93	4.801 (VL)	431.97	3.269 (LLV)	335.37	5.147 (LVL)		
451.89	5.097 (VL)	446.92	3.625 (LLV)	342.76	5.683 (LVL)		
		431.97	4.015 (LVL)	357.62	6.749 (LVL)		
		446.92	4.380 (LVL)	372.43	7.789 (LVL)		
		427.06	4.826 (LL)	387.32	8.810 (LVL)		
		431.97	5.066 (LL)	402.15	9.796 (LVL)		

Table 7
Experimental bubble point (VL), cloud point (LL), phase boundary vapor–liquid to liquid–liquid–vapor (LLV) and phase boundary liquid–liquid–vapor to liquid–liquid (LVL) data for $w_1 \cdot CO_2 + (1 - w_1)[w_2 \cdot HPG(18,000\,g/mol) + w_3 \cdot CH_3OH]$ at various mass fractions w_1 of CO_2, for $w_2 = 0.250$ and $w_3 = 0.750$.

$w_1 = 0.021$		$w_1 = 0.049$		$w_1 = 0.102$		$w_1 = 0.151$	
T (K)	P (MPa)	T (K)	P (MPa)	T (K)	P (MPa)	T (K)	P (MPa)
327.88	0.651 (VL)	312.11	1.167 (VL)	312.08	2.297 (VL)	311.99	4.665 (LVL)
342.75	0.826 (VL)	326.86	1.377 (VL)	326.77	2.887 (VL)	319.34	5.256 (LVL)
350.23	0.927 (VL)	341.65	1.597 (VL)	341.43	3.523 (VL)	326.59	5.896 (LVL)
357.63	1.037 (VL)	348.75	1.714 (VL)	348.57	3.837 (VL)	341.11	7.222 (LVL)
372.43	1.287 (VL)	356.38	1.833 (VL)	356.09	4.108 (LLV)	348.53	7.867 (LVL)
387.33	1.592 (VL)	371.12	2.088 (VL)	363.35	4.337 (LLV)	355.54	8.548 (LVL)
402.17	1.968 (VL)	385.89	2.348 (VL)	370.73	4.499 (LLV)	370.20	9.828 (LVL)
417.08	2.439 (VL)	400.53	2.449 (VL)	378.11	4.663 (LLV)	377.58	10.395(LVL)
431.97	3.014 (VL)	415.15	2.639 (VL)	385.45	4.745 (LLV)	384.86	11.039(LVL)
439.46	3.355 (VL)	422.34	2.949 (VL)	400.12	4.807 (LLV)		
446.90	3.735 (VL)	427.28	3.269 (LLV)	414.94	4.664 (LLV)		
		429.85	3.625 (LLV)	422.24	4.519 (LLV)		
		444.50	4.015 (LLV)	356.09	4.188 (LVL)		
		427.24	4.380 (LVL)	363.31	4.512 (LVL)		
		429.89	4.826 (LVL)	370.73	4.864 (LVL)		
		444.54	50.66 (LVL)	378.11	5.208 (LVL)		
		427.27	5.046 (LL)	385.47	5.554 (LVL)		
		429.85	4.861 (LL)	400.16	6.167 (LVL)		
		444.53	4.677 (LL)	414.86	6.982 (LVL)		
				422.19	7.340 (LVL)		
				429.66	7.727 (LVL)		
				444.34	8.508 (LVL)		
				356.06	4.788 (LL)		
				363.35	5.748 (LL)		
				370.72	7.165 (LL)		
				378.11	8.350 (LL)		
				385.44	9.882 (LL)		

of the hyperbranched polymer was mentioned above as a possible explanation for the upward trend of the bubble point pressure with increasing polymer molar mass (compare Fig. 5). Structural variations were also found for model dendrimers by molecular simulation [34]. Any such effect is not captured by the model because the theory does not adequately account for intramolecular interactions. Chapman et al. have shown that intramolecular association has a strong influence on the phase behavior [35]. In our previous study [11] we further argue that the effect of branching leads to a significant contribution in the dispersive interactions of these polymers. The relation between intra- and intermolecular interactions changes with varying composition, temperature, and pressure for highly branched structures, which, in turn, is relevant for the thermodynamic properties of these substances and their mixtures.

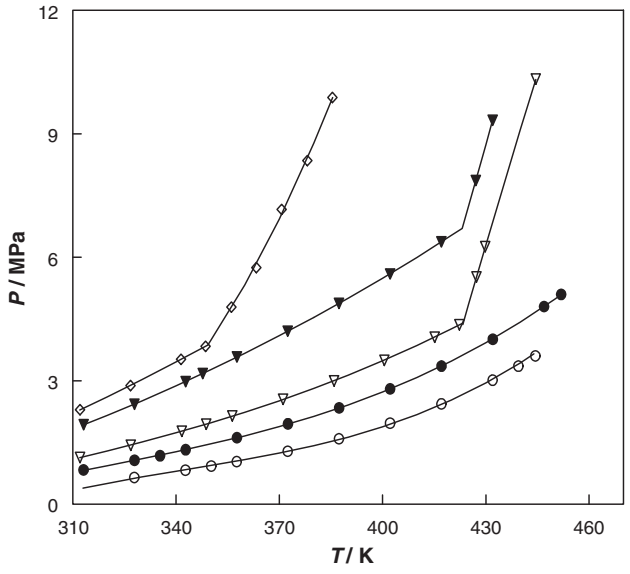

Fig. 4. Influence of polymer concentration on the phase behavior of hyperbranched PG (18,000 g/mol) + methanol + CO_2, with $w_{CO_2} = 0.02$ (*circles*), $w_{CO_2} = 0.05$ (*triangles*), and $w_{CO_2} = 0.10$ (*diamonds*), open symbols $w_{CO_2} \cdot CO_2 + (1 - w_{CO_2})$ [25 mass-% hyperbranched PG + 75 mass-% methanol] and closed symbols $w_{CO_2} \cdot CO_2 + (1 - w_{CO_2})$ [50 mass-% hyperbranched PG + 50 mass-% methanol]. The lines are a guide for the eye.

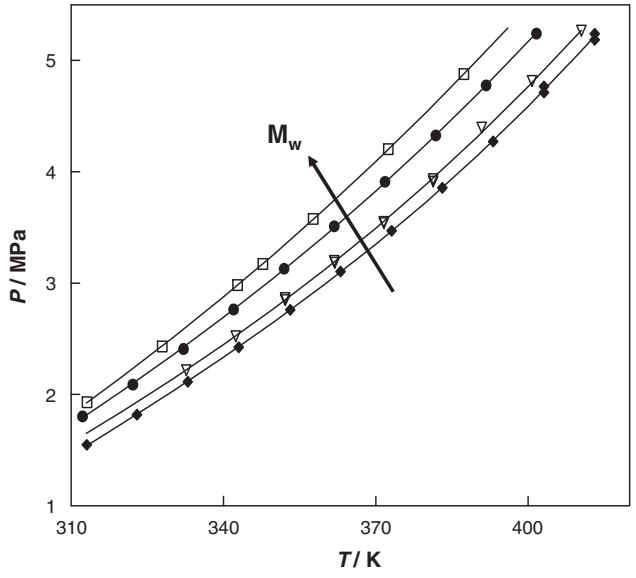

Fig. 5. Bubble point curves of the ternary system $(1 - w_{CO_2})$[50 mass-% hyperbranched PG + 50 mass-% methanol] and CO_2, with $w_{CO_2} = 0.05$. The molar mass of the hyperbranched PG is varying; $M_w = 2700$ g/mol (*diamonds*), $M_w = 5700$ g/mol (*open triangles*), $M_w = 10,000$ g/mol (*circles*), and $M_w = 18,000$ g/mol (*open squares*). Data for $M_w = 2700$ g/mol is taken from Ref. [11]. The lines are a guide for the eye.

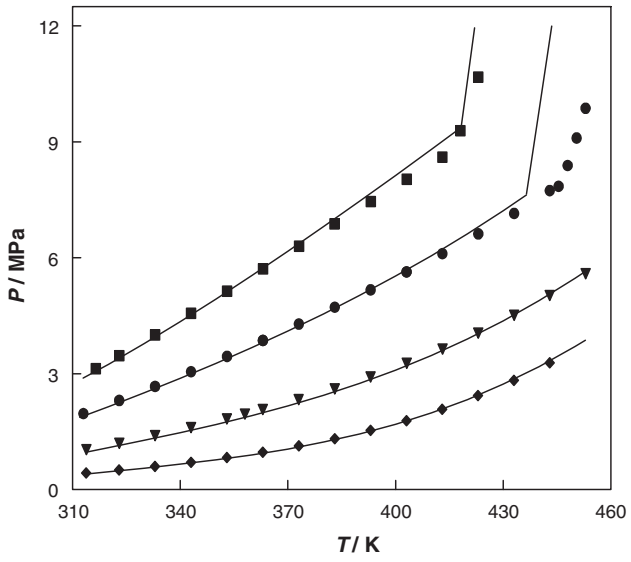

Fig. 6. Bubble point and dew point curves of the ternary system $(1 - w_{CO_2})$[25 mass-% hyperbranched PG (2700 g/mol) + 75 mass-% methanol] and CO_2, with $w_{CO_2} = 0.02$ (*diamonds*), $w_{CO_2} = 0.05$ (*triangles*), $w_{CO_2} = 0.10$ (*circles*) and $w_{CO_2} = 0.15$ (*squares*). Comparison of experimental PCP-SAFT correlations to experimental data [11].

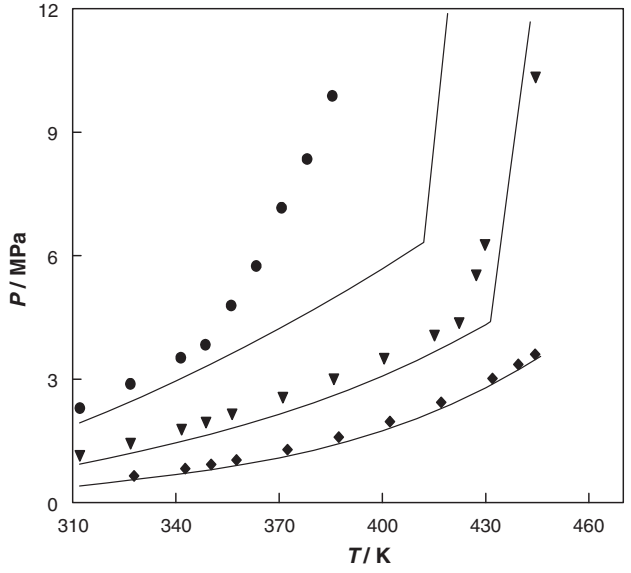

Fig. 7. Bubble point and dew point curves of the ternary system $(1 - w_{CO_2})$[25 mass-% hyperbranched PG (18,000 g/mol) + 75 mass-% methanol] and CO_2, with $w_{CO_2} = 0.02$ (*diamonds*), $w_{CO_2} = 0.05$ (*triangles*) and $w_{CO_2} = 0.10$ (*circles*). Comparison of experimental PCP-SAFT correlations to experimental data (this work).

4. Conclusions

A systematic analysis of the influence of the molar mass of hyperbranched polyglycerol on the phase equilibrium with methanol and carbon dioxide is presented. The system can be classified as a type IV system according to Konynenburg and Scott [24], in which the polymer mass fraction at the lower critical solution temperature unexpectedly exceeds $w_{polymer} = 0.45$. The experimental results show a pronounced dependence of the bubble point pressure on the polymer molar mass, indicating an effect of the polymer structure on the vapor–liquid equilibrium.

The PC-SAFT equation of state can be applied to describe vapor–liquid as well as liquid–liquid phase equilibria of systems including hyperbranched polymers. The description of vapor–liquid–liquid equilibria requires the application of temperature-dependent binary interaction parameters, supporting the hypothesis that structural changes of the hyperbranched polyglycerol (which are not accounted for in the model) occur.

Acknowledgements

The financial support of Shell Global Solutions (Amsterdam) is appreciated. Further, the authors would like to thank Eugene Straver for his constant support with the experimental work.

References

[1] D. Wilms, J. Nieberle, J. Klos, H. Loewe, H. Frey, Chem. Eng. Technol. 30 (2007) 1519–1524.
[2] A. Sunder, J. Heinemann, H. Frey, Chem. Eur. J. 6 (2000) 2499–2506.
[3] A. Striolo, J.M. Prausnitz, A. Bertucco, R.A. Kee, M. Gauthier, Polymer 42 (2001) 2579–2584.
[4] C. Mio, S. Kiritsov, Y. Thio, R. Brafman, J. Prausnitz, C. Hawker, E.E. Malmstrom, J. Chem. Eng. Data 43 (1998) 541–550.
[5] M. Seiler, W. Arlt, H. Kautz, H. Frey, Fluid Phase Equilibr. 201 (2002) 359–379.
[6] M. Seiler, J. Rolker, W. Arlt, Macromolecules 36 (2003) 2085–2092.
[7] M. Seiler, J. Rolker, L. Mokrushina, H. Kautz, H. Frey, W. Arlt, Fluid Phase Equilibr. 221 (2004) 83–96.
[8] M. Seiler, C. Jork, A. Kavarnou, W. Arlt, R. Hirsch, AIChE J. 50 (2004) 3290–13290.
[9] M. Seiler, Fluid Phase Equilibr. 241 (2006) 155–174.
[10] J. Rolker, M. Seiler, L. Mokrushina, W. Arlt, Ind. Eng. Chem. Res. 46 (2007) 6572–6583.
[11] M.K. Kozlowska, B.F. Jurgens, C.S. Schacht, J.T. Gross, W. de Loos, J. Phys. Chem. B 113 (2009) 1022–1029.
[12] K. Inoue, Prog. Polym. Sci. 25 (2000) 453–571.
[13] B.I. Voit, A. Lederer, Chem. Rev. 109 (2009) 5924–5973.
[14] J.G. Lieu, M.J. Liu, J.M.J. Frechet, J.M. Prausnitz, J. Chem. Eng. Data 44 (1999) 613–620.
[15] D. Wilms, S.E. Stiriba, H. Frey, Accounts Chem. Res. 43 (2010) 129–141.
[16] D. Wilms, F. Wurm, J. Nieberle, P. Bohm, U. Kemmer-Jonas, H. Frey, Macromolecules 42 (2009) 3230–3236.
[17] L. Lue, J.M. Prausnitz, Macromolecules 30 (1997) 6650–6657.
[18] J.G. Jang, Y.C. Bae, J. Chem. Phys. 114 (2001) 5034–5042.
[19] J.G. Jang, Y.C. Bae, Chem. Phys. 269 (2001) 285–294.
[20] J.G. Jang, Y.C. Bae, J. Chem. Phys. 116 (2002) 3484–3492.
[21] T. Zeiner, D. Browarzik, S. Enders, Fluid Phase Equilibr. 286 (2009) 127–133.
[22] T.W. de Loos, H.J. van der Kooi, P.L. Ott, J. Chem. Eng. Data 31 (1986) 166–168.
[23] M.H. ter Horst, S. Behme, G. Sadowski, T.W. de Loos, J. Supercrit. Fluids 23 (2002) 181–194.
[24] P.H.V. Konynenburg, R.L. Scott, Phil. Trans. R. Soc. Lond. A 298 (1980) 495–540.
[25] J.M. Prausnitz, R.N. Lichtenthaler, E. Gomes de Azevedo, Molecular Thermodynamics of Fluid-phase Equilibria, 3rd ed., Prentice Hall PTR, New Jersey, 1999.
[26] L. Vanopstal, R. Koningsveld, Polymer 33 (1992) 3433–3444.
[27] J. Gross, G. Sadowski, Fluid Phase Equilibr. 168 (2000) 183–199.
[28] J. Gross, G. Sadowski, Ind. Eng. Chem. Res. 40 (2001) 1244–1260.
[29] J. Gross, G. Sadowski, Ind. Eng. Chem. Res. 41 (2002) 5510–5515.
[30] J. Gross, AIChE J. 51 (2005) 2556–2568.
[31] J. Gross, J. Vrabec, AIChE J. 52 (2006) 1194–1204.
[32] J. Gross, G. Sadowski, Ind. Eng. Chem. Res. 41 (2002) 1084–1093.
[33] J. Gross, O. Spuhl, F. Tumakaka, G. Sadowski, Ind. Eng. Chem. Res. 42 (2003) 1266–1274.
[34] P. Carbone, F. Negri, F. Müller-Plathe, Macromolecules 40 (2007) 7044–7055.
[35] W.G. Chapman, S.G. Sauer, D. Ting, A. Ghosh, Fluid Phase Equilibr. 217 (2004) 137–143.